M2-TAM-derived exosomal miR-491-3p modulates UBE2D3 and promotes the proliferation, migration and invasion of lung cancer cells

QIANG ZHANG[1-3], YUNGANG SUN[1-3], YU ZHUANG[1-3], SHIWEI XU[4], MENGXU YAO[1-3], SIYANG JIAO[1-3], QI WANG[1-3], FENG SHAO[1-3] and XIAOYING ZHANG[5]

[1]Department of Thoracic Surgery, Nanjing Chest Hospital, Nanjing, Jiangsu 210029, P.R. China; [2]Department of Thoracic Surgery, Affiliated Nanjing Brain Hospital, Nanjing Medical University, Nanjing, Jiangsu 210029, P.R. China; [3]Pulmonary Nodule Diagnosis and Treatment Research Center, Nanjing Medical University, Nanjing 210029, P.R. China; [4]Wuxi School of Medicine, Jiangnan University, Wuxi 214000, P.R China; [5]The Third Affiliated Hospital of Soochow University, Tianning, Changzhou, Jiangsu 215004, P.R. China

Received February 4, 2026; Accepted May 29, 2026

DOI: 10.3892/or.2026.9164

Abstract. M2 tumor-associated macrophages (M2-TAMs) have been reported to promote tumor growth through exosome-dependent mechanisms. However, the exact role of exosomes derived from M2-TAMs (M2-TAM-Exos) in lung cancer progression remains unclear. In The present study, M2-like macrophages (IL-4/IL-13-polarized THP-1-derived macrophages) were shown to release exosomes that lung cancer cells effectively internalized. These exosomes markedly enhanced the proliferation, migration, and invasion of lung cancer cells, thereby promoting malignancy. Further analyses revealed that M2-like macrophage-derived exosomes contain high levels of microRNA (miR)-491-3p. *In vitro* and *in vivo* experiments confirmed miR-491-3p as an oncogenic miR, while its inhibition markedly reduced cancer cell aggressiveness. Additional experiments demonstrated that miR-491-3p suppressed UBE2D3 expression after entering lung cancer cells. Collectively, these findings suggest a model in which M2-like macrophages deliver miR-491-3p via exosomes to downregulate UBE2D3, facilitating lung cancer progression.

Correspondence to: Professor Feng Shao, Department of Thoracic Surgery, Nanjing Chest Hospital, 215 Guangzhou Road, Nanjing, Jiangsu 210029, P.R. China
E-mail: doctorshao1982@sina.com

Professor Xiaoying Zhang, The Third Affiliated Hospital of Soochow University, 185 Bureau Front Street, Tianning, Changzhou, Jiangsu 215004, P.R. China
E-mail: zhangxy1159966@163.com

Key words: M2 tumor-associated macrophages, exosomes, microRNA, ubiquitin conjugating enzyme E2 D3, lung cancer

Introduction

Cancer is a complex disease characterized by uncontrolled proliferation, immune evasion, and a strong propensity for invasion and metastasis (1,2). Increasing evidence suggests that heterogeneity within the tumor microenvironment (TME) markedly and variably influences malignant progression (3,4). The TME is a dynamic and complex ecosystem that initially functions as a vigilant sentinel during early tumor stages. At this stage, immune cells, fibroblasts and extracellular matrix components collaborate to inhibit neoplastic growth (5,6). Paradoxically, as carcinogenesis advances, these formerly protective elements transform into key facilitators of tumor progression (7). Consequently, therapeutic strategies targeting the reconfiguration of the TME have emerged as promising approaches in cancer treatment.

Within the cellular components of the TME, macrophages represent the predominant immune infiltrates. Rather than inhibiting cancer, these macrophages frequently adopt a phenotype supportive of tumor progression. The alternatively activated M2 subtype particularly coordinates angiogenesis, metastasis, chemoresistance, and systemic immunosuppression (8-10). Nevertheless, the exact molecular mechanisms by which M2-TAMs communicate with lung cancer cells remain incompletely defined. Thus, clarifying this intercellular signaling pathway is crucial for developing macrophage-targeted therapies for lung cancer.

Exosomes, nanoscale extracellular vesicles carrying complex assortments of RNAs and proteins, serve as ubiquitous intercellular messengers. They regulate critical functions in both physiological and pathological states (11-13). In cancer, exosome-mediated communication orchestrates transcriptional networks that coordinate interactions between malignant cells and stromal components. This influences proliferative capacity, metastatic potential, immune evasion and therapeutic resistance (14). Exosomal bioactive cargo, such as proteins, microRNAs (miRNAs/miRs), long non-coding (lnc)RNAs and circular (circ)RNAs, enables diverse biological activities (15). For instance, exosomal lncRNAs from various donor cells

are causally linked to cancer pathogenesis and therapeutic response (12,16). It has been demonstrated that exosomes act as crucial conduits for bidirectional communication between tumor cells and macrophages (17); however, the molecular mechanisms underlying this crosstalk remain poorly defined. An in-depth investigation of exosome-mediated intercellular communication between tumor cells and macrophages will enhance the understanding of TME regulation and provide a basis for therapeutic strategies aimed at exosome inhibition, immune reactivation, metastasis suppression, and overcoming chemoresistance.

The present study identified a previously unrecognized communication pathway between M2-like macrophages and lung cancer cells within the TME. Functional analyses demonstrated that M2-like macrophages facilitate lung cancer progression through the paracrine secretion of exosomes. Furthermore, inhibiting exosome secretion using GW4869 markedly impeded lung cancer development. Mechanistically, M2-like macrophage-derived exosomes contain abundant miR-491-3p, which is horizontally transferred to lung cancer cells and acts as a potent oncogenic microRNA (oncomiR). Specific inhibition of miR-491-3p effectively attenuated cancer cell aggressiveness. After uptake by cancer cells, miR-491-3p directly suppressed UBE2D3 expression, thereby activating oncogenic pathways that promote proliferation, migration, and invasion. The present study elucidated an exosome-mediated molecular mechanism by which M2-like macrophages drive lung cancer cells toward a more aggressive phenotype. These findings enhance the understanding of lung cancer pathogenesis and highlight the M2-TAM-exosome-miR-491-3p-UBE2D3 axis as a promising therapeutic target for lung cancer intervention.

Materials and methods

Ethical approval. Tumor and adjacent normal tissues (>3 cm away from the edge of the tumor lesion) were collected from patients with lung cancer at the Department of Thoracic Surgery, Nanjing Chest Hospital (Jiangsu, China) between January 1, 2023, and May 31, 2023. Of the 68 patients, 32 were male and 36 were female; patient ages ranged from 46-84 years, with a median age of 65.5 years. The histological types, staging, treatment status and other information for the 68 paired patient samples are shown in Table SI. Informed consent was obtained from all participants. The study received approval from the Institutional Review Board of Nanjing Chest Hospital (approval no. 2023-KL034-01) and complied with all relevant ethical guidelines.

Inclusion criteria for the 68 patients were: i) Age range 18–84 years; ii) initial diagnosis of lung cancer (no particular pathogenic type indicated); iii) no prior antineoplastic therapy prior to surgical intervention; iv) good surgical tolerance with no contraindications; v) capable of regular follow-up. Patient samples that did not meet the aforementioned criteria were not be included in any experiments described in this manuscript.

Immunohistochemistry. Tissue specimens were embedded in a preheated embedding station with the desired sectioning orientation, subsequently demolded and excess paraffin trimmed off. Paraffin-embedded specimens were sectioned to a thickness of 3 μm. Sections were dewaxed in xylene and sequentially rehydrated through graded ethanol (100, 95 and 75%; 1 min each), followed by rinsing in distilled water for 5 min. Endogenous peroxidase activity was subsequently quenched by incubation with 3% H_2O_2 at room temperature for 10 min. Subsequently, antigen retrieval was performed using citrate buffer in a microwave. The sections were blocked with Immunol Staining Blocking Buffer (Beyotime Biotechnology; cat. no. P0102) at room temperature for 60 min. Samples were incubated overnight at 4˚C with diluted anti-CD68 primary antibody (Abmart Pharmaceutical Technology Co., Ltd.; cat. no. MN50019S; 1:100-1:200). The following day, The sections were incubated with HRP-labeled Goat Anti-Rabbit IgG(H+L) (Beyotime Biotechnology; cat. no. A0208, 1:250) at 37˚C for 60 min. The sections were subsequently incubated with DAB working solution (Dako; Agilent Technologies, Inc.) and monitored microscopically until optimal color development was achieved, followed by immediate rinsing in deionized water. Nuclear counterstaining was performed with Mayer's hematoxylin at 37˚C for 1 min. The slides were then dehydrated in absolute ethanol for 10 sec, air-dried at 55-60˚C and mounted with neutral balsam. The stained sections were finally examined under a light microscope (Carl Zeiss AG).

RNA extraction and quantitative PCR (qPCR). Tissue samples were processed in liquid nitrogen, minced, and ground into a fine powder. Total RNA extraction from tissues was performed using the FastPure Cell/Tissue Total RNA Isolation Kit V2, while RNA from cultured cells was extracted using the RNA Extraction Kit. cDNA synthesis utilized the HIScript III RT SuperMix qPCR Kit (+gDNA Wiper), and quantitative PCR (RT-qPCR) was conducted with ChamQ Universal SYBR qPCR Master Mix. Primers were designed and synthesized by Nanjing Punoen Biological Co., Ltd. The primer sequences are listed in Table SII.

Cell culture. Human lung cancer cell lines A549 and H460 were obtained from Nanjing Punoen Biological Co., Ltd. Cells were cultured in DMEM supplemented with 10% fetal bovine serum (FBS; Gibco; Thermo Fisher Scientific, Inc.) and 1% penicillin/streptomycin. Cells were passaged when reaching ~80% confluence.

Macrophage polarization. THP-1 cells (Nanjing Punoen Biological Co., Ltd.) were seeded in 6-well plates and cultured with 100 nM PMA for 48 h at 37˚C with 5% CO_2. Cells were then incubated with fresh medium (without PMA) for 24 h to establish M0 macrophages. M0 macrophages were subsequently cultured in fresh medium containing polarizing factors (25 ng/ml each of IL-4 and IL-13) for 48 h to obtain M2-like macrophages.

Cellular flow cytometry. The harvested M0 and M2 macrophages were washed twice with PBS and centrifuged (200 x g) at 37˚C for 5 min. Cells were incubated in Fixation/Permeabilization solution (Becton, Dickinson and Company; cat. no. 554722) at room temperature for 20 min, followed by centrifugation (200 x g) at 37˚C for 5 min. Cells underwent two washes with 1X Perm/Wash Buffer (Beyotime

Biotechnology), followed by centrifugation (200 x g) at 37˚C for 5 min. Subsequently, $1x10^6$ cells per tube were incubated with PE anti-CD206 antibody (Fine Test; cat. no. PE-30095) at room temperature in the dark for 30 min. Cells were again washed twice with 1X Perm/Wash Buffer, resuspended in PBS, and analyzed by flow cytometry (CytoFLEX S; Beckman Coulter, Inc.). Flow cytometry data were analyzed using FlowJo software (version 10.8.1; BD Biosciences).

CCK-8 cell proliferation assay. Lung cancer cells were seeded at 1,500 cells per well in 96-well plates with 100 μl complete medium. After cell adhesion, five replicates per group were set up. At days 1, 2, 3 and 4, 10 μl CCK-8 solution was added per well, followed by incubation at 37˚C with 5% CO_2 for 2 h. Absorbance (OD) was measured at 450 nm using a microplate reader, and proliferation curves were plotted.

Colony formation assay. Cells were diluted to 1,000 cells/ml in complete medium and seeded evenly in 6-well plates. After 4-6 h incubation at 37˚C and 5% CO_2 for cell adherence, experimental groups were treated according to the study design and control groups received an equivalent solvent volume. Cells were cultured for 14 days or until the majority of single-cell-derived clones contained >50 cells, with 1 ml medium replaced every 3 days. Following medium removal, plates were washed with PBS, and cells were fixed with 1 ml methanol for 15 min. After fixation, cells were stained with 0.5% crystal violet solution (1 ml per well) for 10 min at room temperature. Excess dye was rinsed with running water, plates were air-dried, and colony numbers were quantified microscopically using image analysis.

Cell migration. Lung cancer cells ($5x10^4$ cells per well) suspended in serum-free medium were seeded in the upper chamber (Corning, Inc.). Medium containing 10% FBS was added to the lower chamber. After 24-72 h incubation, non-migrating cells in the upper chamber were removed. At room temperature, cells adhering to the lower chamber were fixed with 4% paraformaldehyde for 30 min, stained with Crystal Violet staining solution for 6 min and quantified through inverted fluorescence microscope (IX83; Olympus Corporation) and image analysis (GraphPad Prism 9.0; Dotmatics).

Cell invasion. Matrigel was diluted 1:15 in serum-free medium. A total of 100 μl was added to the upper chamber (Corning, Inc.) and incubated at 37˚C in a cell culture hood overnight. Excess medium was aspirated before use. Lung cancer cells ($8x10^4$ cells per well) suspended in serum-free medium were seeded in the upper chamber. Medium containing 10% FBS was added to the lower chamber. After 24-72 h incubation, non-migrating cells in the upper chamber were removed. At room temperature, cells adhering to the lower chamber were fixed with 4% paraformaldehyde for 30 min, stained with Crystal Violet staining solution for 6 min and quantified through inverted fluorescence microscopy (OLYMPUS IX83) and image analysis (GraphPad Prism 9.0).

Animal studies. Animal experiments were approved by the Animal Ethics Committee of Jiangnan University [approval no. JN.No20241230b0200211(715)]. Male C57BL/6 and BALB/c nude mice (6-8 weeks old; n=25) were purchased from Shanghai Nanfang Model Biotechnology Co., Ltd., and housed under pathogen-free conditions at 21-26˚C and 50-60% relative humidity, with a 12-h light/dark cycle (15-20 lux). After a one-week acclimation, mice were randomly assigned to experimental groups.

Lung cancer cells in logarithmic growth were harvested, centrifuged (200 x g) at 37˚C for 5 min, and resuspended in a 1:1 mixture of culture medium and Matrigel at a concentration of $1x10^6$ cells/100 μl. Cell suspensions were injected subcutaneously into the axillary region of mice. Tumor volumes were measured at 7, 14, 21 and 28 days post-inoculation. At study termination, mice were sacrificed, tumors excised, images captured and the tumors fixed in 4% paraformaldehyde for 24 h. Maximum tumor diameter was 0.99 cm, and maximum tumor volume was 395 mm^3.

The specific sacrifice procedure for mice was as follows: Mice were administered an intraperitoneal injection of pentobarbital sodium (150 mg/kg). Following injection, respiratory movements were continuously monitored. At two min after the cessation of respiration, the cornea was gently touched to assess the absence of the blink reflex. Mortality was subsequently confirmed by cervical dislocation as a secondary verification measure.

Exosome extraction and identification. After successful polarization of M0 and M2-like macrophages, cells were incubated in serum-free RPMI-1640 medium for 24 h at 37˚C. Culture supernatants were collected, and exosomes were isolated by ultracentrifugation at 4˚C as follows: 1,000 x g for 10 min, 3,000 x g for 30 min, and 10,000 x g for 60 min. Supernatants were then filtered through a 0.22 μm membrane and ultracentrifuged at 100,000 x g for 2 h. Pelleted exosomes were resuspended in PBS and stored at -80˚C.

Transmission Electron Microscope (TEM). Specimens were applied to copper grids (Beijing Zhongjixinke Scientific Instrument Co., Ltd.; cat. no. AZH200), allowed to adsorb onto the grids at room temperature. Copper grids were stained with uranyl acetate (Electron Microscopy Sciences; cat. no. 22400) at room temperature for 5 min, and subsequently examined by TEM (JEOL Ltd.; JEM-1400), Representative TEM images revealed the characteristic morphology typical of exosomes.

Nanoparticle tracking analysis (NTA). NTA with Zetaview-PMX120-Z (Particle Metrix GmbH) and corresponding software ZetaView (version 8.05.14 SP7). Isolated exosome samples were appropriately diluted using 1X PBS buffer (Beyotime Biotechnology) to measure the particle size and concentration. NTA measurement was recorded and analyzed at 11 positions. The ZetaView system was calibrated using 100 nm polystyrene particles. Temperature was maintained at 23˚C and 30˚C.

Bicinchoninic Acid Assay (BCA) assay. The BCA working reagent was prepared by mixing Reagent A and Reagent B from the BCA Protein Assay Kit (Biosharp Life Sciences; cat. no. BL521S;) at a 50:1 volume ratio. BSA standards were prepared according to the manufacturer's instructions, and

varying volumes of standards and test samples were dispensed into a 96-well microplate. Subsequently, 200 μl of the working reagent was added to each well, mixed thoroughly, and the plate was incubated at 37˚C for 30 min. Absorbance at 562 nm was then measured using a microplate reader (Thermo Fisher Scientific, Inc.) and the optical density values were recorded.

Particle size was assessed by nanoparticle tracking analysis (NTA) and protein concentration was measured using a BCA assay. The particle concentration was $6.4x10^{10}$ particles/ml, as indicated by these results. Additionally, BCA protein assays indicated a protein content of 60 μg/ml. The Particle-to-Protein Ratio for the extracted exosomes is $1.07x10^{9}$ particles/μg, thereby affirming that the purity of the experimental materials adheres to the requisite requirements. Finally, Following exosome isolation, the expression of exosomal marker proteins was assessed by western blotting. The extracts were positive for the exosomal markers CD81, CD63 and TSG101, and negative for GM130, a negative control. The aforementioned identification methods and results satisfy criteria a, b, and c outlined (Steps of EV Characterization) of the MISEV2018 guidelines (18). It was hypothesized that it was appropriate to characterize this extract as exosomes.

Exosomes labelling. The fluorescent dye Dil (MCE; cat. no. HY-D0083) was dissolved in DMSO to create a 1 mg/ml stock solution, diluted 1:100 with PBS to prepare a working solution. PBS and isolated exosomes were each mixed 1:1 with the Dil working solution, incubated at 37˚C for 30 min, and then washed with PBS. The mixtures were processed following the same procedure used for exosome extraction to collect labelled exosomes. Finally, Dil-labelled exosomes were resuspended in PBS and stored at -80˚C for subsequent experiments.

Exosome internalization assay. A549 and H460 cells were cultured overnight at 37˚C in 24-well plates. Dil dye and Dil-labelled exosomes were diluted in RPMI-1640 medium, evenly distributed into the wells, and incubated under light-protected conditions for 12 h. At room temperature, cells were then fixed in 4% paraformaldehyde for 30 min, stained with DAPI for 10 min, mounted on slides, and imaged using confocal microscopy.

Plasmid transfection. The 3rd generation A549 and H460 cells were seeded in 6-well plates and incubated overnight at 37˚C with 5% CO_2. On the following day, 200 μl OMEM, 6 μl REVG007 transfection reagent, and 2 μg plasmid were added per well according to the manufacturer's instructions. Cells were incubated for an additional 48 h, then harvested and divided for subsequent western blotting and qPCR. The UBE2D3 knockdown plasmid, REVG007 transfection reagent, and OMEM were purchased from Shanghai Genechem Co., Ltd.. Relevant short hairpin (sh)RNA sequences were: sh-UBE2D3: CCCATATCAAGGCGGTGTATT; sh-negative control (NC): TTCTCCGAACGTGTCACGT.

Western blotting. Total proteins were extracted from tissues or cells using RIPA lysis buffer (Beyotime Biotechnology; cat. no. P0013B) and quantified. Samples (10 μg protein per lane) were separated by electrophoresis on a 10% SDS-polyacrylamide gel, transferred onto a PVDF membrane, and blocked with 5% skimmed milk at room temperature for 1 h. Membranes were incubated overnight at 4˚C with primary antibodies (Abmart Pharmaceutical Technology Co., Ltd.; CD81, cat. no. T55742S; CD63, cat. no. TR19741S; TSG101, cat. no. T55985S; UBE2D3, cat. no. TB6189S and β-actin, cat. no. P30002S; all diluted 1:2,000). After washing, membranes were incubated with HRP-labeled Goat Anti-Rabbit IgG(H+L) (Beyotime Biotechnology; cat. no. A0208; 1:1,000) at room temperature for 1 h. Bands were visualized using a BeyoECL Plus (Beyotime Biotechnology; cat. no. P0018S). Chemiluminescent signals were detected using a ChemiDoc Touch Imaging System (Bio-Rad Laboratories, Inc.).

Cell transfection. Lung cancer cells were harvested by digestion with 0.25% trypsin the day before transfection. Cells were seeded ($3x10^{5}$ cells/well) in 6-well plates with 2 ml complete medium and incubated overnight at 37˚C. For each well, 20 pmol antagomiR-NC and antagomiR-491-3p (Sangon Biotech) was diluted in 50 μl serum-free RPMI-1640 medium. Additionally, 1 μl Lipofectamine® 2000 reagent (Invitrogen; Thermo Fisher Scientific, Inc.) was diluted in 50 μl serum-free RPMI-1640 medium, then incubated for 5 min at room temperature. The diluted solutions were combined, mixed gently, and incubated for 20 min at room temperature to form complexes. After washing twice with PBS, each well received 2 ml serum-free medium, and complexes were added dropwise. Plates were gently shaken and incubated for 24-72 h, with fresh complete medium replaced every 4-6 h, depending on cell viability. Subsequent related experiments were performed after incubation for 72 h. Relevant antagomiRNA sequences were: antagomiR-NC: ACAGUAACUUGCGUGAUUAUUG; antagomiR-491-3p: GUAGAAGGGAAUCUUGCAUAAG.

Statistical analysis. All biological experiments included three independent repeats (n=3), each comprising three technical replicates. Statistical analyses were performed using GraphPad Prism 9.0 (Dotmatics) and SPSS 22.0 software (IBM Corp.), with data presented as mean ± standard deviation. Differences between two groups were compared using unpaired Student's t-test and comparisons among three or more groups were performed with one-way or two-way ANOVA followed by Tukey's post hoc test for multiple comparisons. $P<0.05$ was considered to indicate a statistically significant difference.

Results

M2-TAMs are markedly increased in lung cancer tissues. To investigate the role of macrophages in lung carcinogenesis and progression, immunostaining for CD68 was performed on 68 pairs of human lung cancer and adjacent normal lung tissues (Fig. 1A and B). The CD68-positive area fraction was markedly greater in tumor tissues compared with adjacent normal tissues (Fig. 1C). Furthermore, analysis of metastatic and non-metastatic lung cancer tissues revealed a higher CD68-positive area fraction in metastatic lesions, indicating increased macrophage infiltration (Fig. 1D). A receiver operating characteristic (ROC) curve analysis demonstrated that the area under the curve (AUC) for CD68 expression in lung cancer was 0.8415, confirming its diagnostic value for lung cancer patients (Fig. 1E). qPCR showed significant upregulation of the M2 macrophage markers ARG1 and IRF4 in tumor

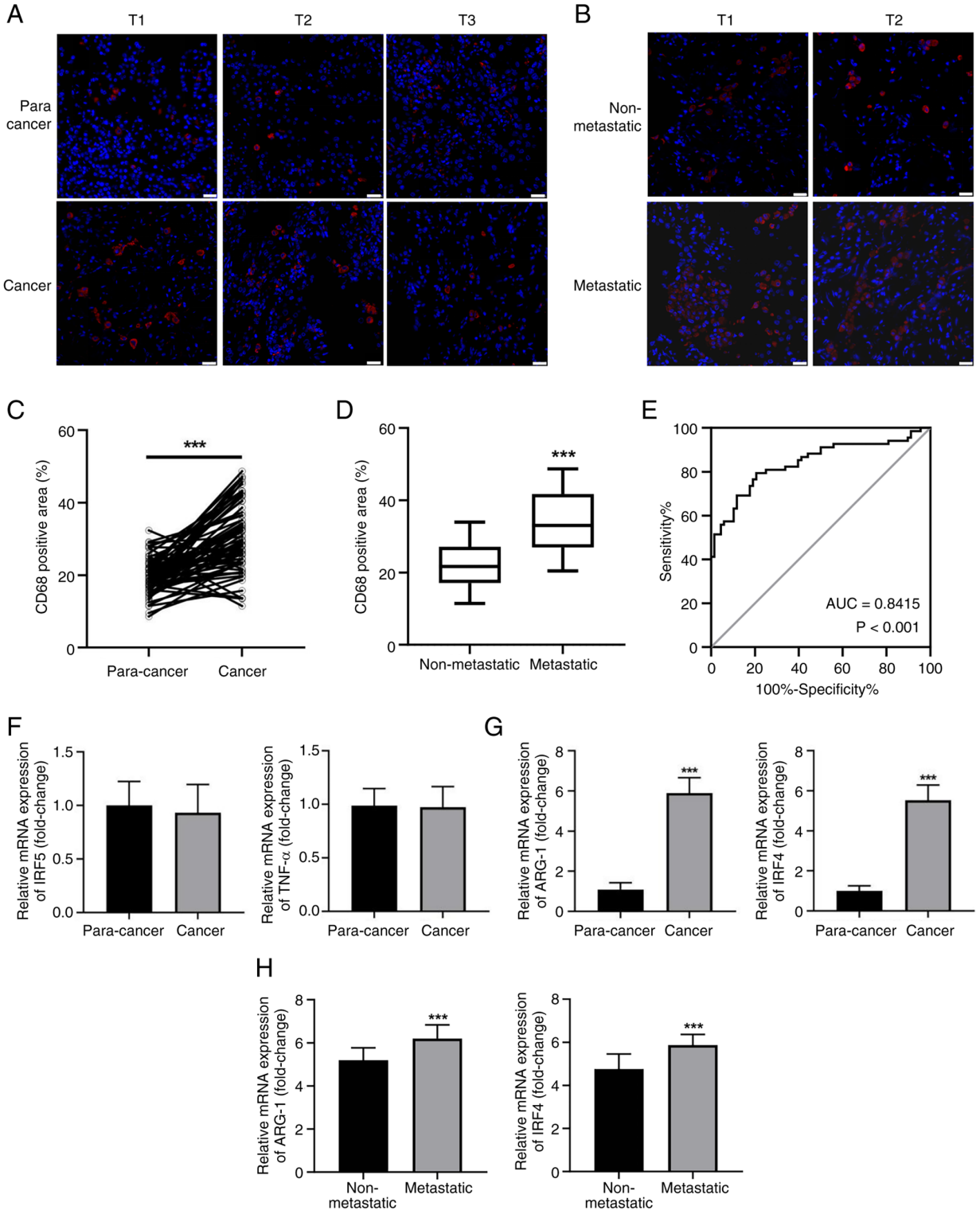

Figure 1. M2-TAMs are markedly increased in lung cancer tissues. (A) Representative images of CD68 immunohistochemical staining in lung cancer and adjacent normal tissues. Scale bar, 50 μm. (B) Representative images of CD68 immunohistochemical staining in non-metastatic and metastatic lung cancer tissues. Scale bar, 50 μm. (C) Statistical comparison of CD68-positive areas between lung cancer tissues and adjacent normal tissues. (D) Statistical analysis of CD68-positive areas between non-metastatic and metastatic lung cancer tissues. (E) ROC curve analysis for CD68 in lung cancer tissues. (F) mRNA expression levels of M1 macrophage markers (IRF5 and TNF-α) in lung cancer tissues compared with adjacent normal tissues. (G) mRNA expression levels of M2 macrophage markers (ARG1 and IRF4) in lung cancer and adjacent normal tissues. (H) mRNA expression levels of M2 macrophage markers (ARG1 and IRF4) in non-metastatic and metastatic lung cancer tissues. Data are presented as mean ± SD. ***P<0.001. M2-TAMs, M2 tumor-associated macrophages; ROC, receiver operating characteristic.

tissues (Fig. 1G), while the M1 markers IRF5 and TNF-α did not exhibit significant differences (Fig. 1F). Additionally, ARG1 and IRF4 expression levels were further elevated in metastatic tissues (Fig. 1H). Collectively, these results indicated that M2-polarized macrophages promoted malignant progression and metastasis in lung cancer.

M2-like macrophages promote proliferation, migration, and invasion of lung cancer cells. THP-1 cells were induced into M0 macrophages and subsequently polarized into M2-like macrophages using cytokines IL-4 and IL-13. Polarization was confirmed by flow cytometry analysis of CD206 expression (Fig. 2A). Concurrently, expression levels of the hallmark M2 markers ARG1 and IRF4 were examined. Results showed markedly increased expression of these markers in M2-like macrophages compared with control cells (Fig. 2B). Conditioned medium (CM) from M2-like macrophages was added to the culture medium of lung cancer cells (A549 and H460) to evaluate its effect. Compared with control groups, the proliferation capacity of cancer cells was markedly enhanced by M2-CM treatment (Fig. 2C). Colony formation assays demonstrated a marked increase in tumor cell clones in the M2-CM groups compared with controls (Fig. 2D). Transwell assays further indicated that the migration and invasion capabilities of tumor cells were markedly enhanced in the M2-CM-treated groups (Fig. 2E-H). *In vivo* studies validated these findings. Control and M2-CM-treated A549 cells were injected into the axillary regions of nude mice. Tumor volume and weight in the M2-CM group were markedly increased compared with controls (Fig. 2I-K). These results demonstrate that conditioned media (CM) from M2-like macrophages markedly promote lung cancer cell proliferation both *in vitro* and *in vivo*.

M2-like macrophages facilitate proliferation, migration, and invasion of lung cancer cells via exosomes. Exosomes, as critical mediators of intercellular communication, markedly contribute to lung cancer progression. To investigate exosome-mediated communication between M2-like macrophages and lung cancer cells, exosomes were isolated from the culture medium of M2-like macrophages by ultracentrifugation and visualized using TEM (Fig. 3A). NTA indicated that exosome diameters ranged mainly from 100-200 nm (Fig. 3B). Western blot analyses confirmed the presence of CD81, CD63 and TSG101 proteins in exosomes but not in whole-cell lysates. By contrast, GM130 protein was absent in exosomes and present in whole-cell lysates (Fig. 3C).

To further explore the role of exosomes, M2-like macrophages were treated with the exosome secretion inhibitor GW4869. Lung cancer cells treated with CM from GW4869-treated macrophages showed markedly reduced proliferation compared with untreated controls (Fig. 3D). Colony formation assays indicated that GW4869 markedly reduced lung cancer cell clonogenicity (Fig. 3E). Transwell assays showed that GW4869 markedly suppressed lung cancer cell migration and invasion (Fig. 3F and G). *In vivo* studies further demonstrated that tumors derived from GW4869-treated cells had markedly lower weights and volumes compared with the untreated M2-CM group (Fig. 3H-J). These results confirmed that M2-like macrophages promote lung cancer malignancy via exosome secretion, and inhibition of exosome release effectively impedes tumor progression.

M2-like macrophages release exosomes enriched in miR-491-3p that affect lung cancer cells. Differentially expressed miRNAs associated with lung cancer progression were identified using the GEO database, revealing miR-20a, miR-21, miR-454, miR-491-3p, miR-140-3p and miR-221 as potential targets (Fig. 4A). qPCR analysis showed that miR-491-3p exhibited the greatest differential expression between control (medium-only) and M2-like macrophage exosome groups (Fig. 4B). miR-491-3p was barely detectable in control (medium-only) groups but was markedly enriched in M2-like macrophage exosomes isolated by the same ultracentrifugation protocol, indicating that miR-491-3p originated from M2-like macrophage exosomes rather than the cell culture medium. Cellular expression analysis further confirmed markedly elevated miR-491-3p levels in both A549 and H460 cells compared with controls (Fig. 4C). Moreover, treatment with M2-like macrophage-derived exosomes markedly increased both precursor and mature miR-491-3p expression in lung cancer cells, indicating direct delivery and induction of miR-491-3p synthesis following exosome internalization (Fig. 4D).

To verify exosome uptake by lung cancer cells, cells were incubated separately with Dil dye alone or with Dil-labeled exosomes. Results indicated that Dil dye alone was not internalized by A549 or H460 cells, whereas Dil-labeled exosomes were efficiently internalized by both cell lines (Fig. 4E). Collectively, these findings demonstrated that M2-like macrophages release exosomes enriched in miR-491-3p, which upon uptake by lung cancer cells, trigger signaling changes that promote lung cancer progression.

Inhibition of miR-491-3p attenuates lung cancer progression. To verify the critical regulatory role of miR-491-3p in lung cancer progression, antagomiR-491-3p was transfected into A549 and H460 cells to reduce miR-491-3p expression (Fig. 5A). Compared with the control group, cell proliferation markedly decreased in the antagomiR-491-3p group (Fig. 5B). Likewise, reduced miR-491-3p expression markedly diminished the colony-forming capability of A549 and H460 cells (Fig. 5C). Transwell assays showed markedly reduced migration and invasion abilities in lung cancer cells following antagomiR-491-3p treatment (Fig. 5D-F). Subsequent *in vivo* studies demonstrated that tumor masses were markedly smaller in both weight and volume in the antagomiR-491-3p-treated group compared with the control group (Fig. 5G). Collectively, these findings indicate that miR-491-3p is critical for lung cancer growth, and its inhibition effectively suppresses malignant behaviors.

miR-491-3p promotes lung cancer progression by inhibiting UBE2D3 expression. To clarify the molecular mechanism by which miR-491-3p facilitates lung cancer progression, downstream targets of miR-491-3p were identified (Table I). UBE2D3, AZI2 and PTPRM emerged as candidate genes for further evaluation. Their expression levels were assessed in HBE135-E6E7, A549 and H460 cells. The results showed that UBE2D3 expression was decreased in tumor cells, while AZI2 and PTPRM were increased (Fig. 6A). Given that miR-491-3p reduces the expression of its target gene upon entering lung cancer cells, UBE2D3 was selected for further analysis. Western blotting confirmed lower UBE2D3 protein expression in A549 and H460 cells (Fig. 6B). qPCR analysis of 68 paired clinical lung cancer samples demonstrated markedly reduced UBE2D3 expression in tumor tissues compared with adjacent

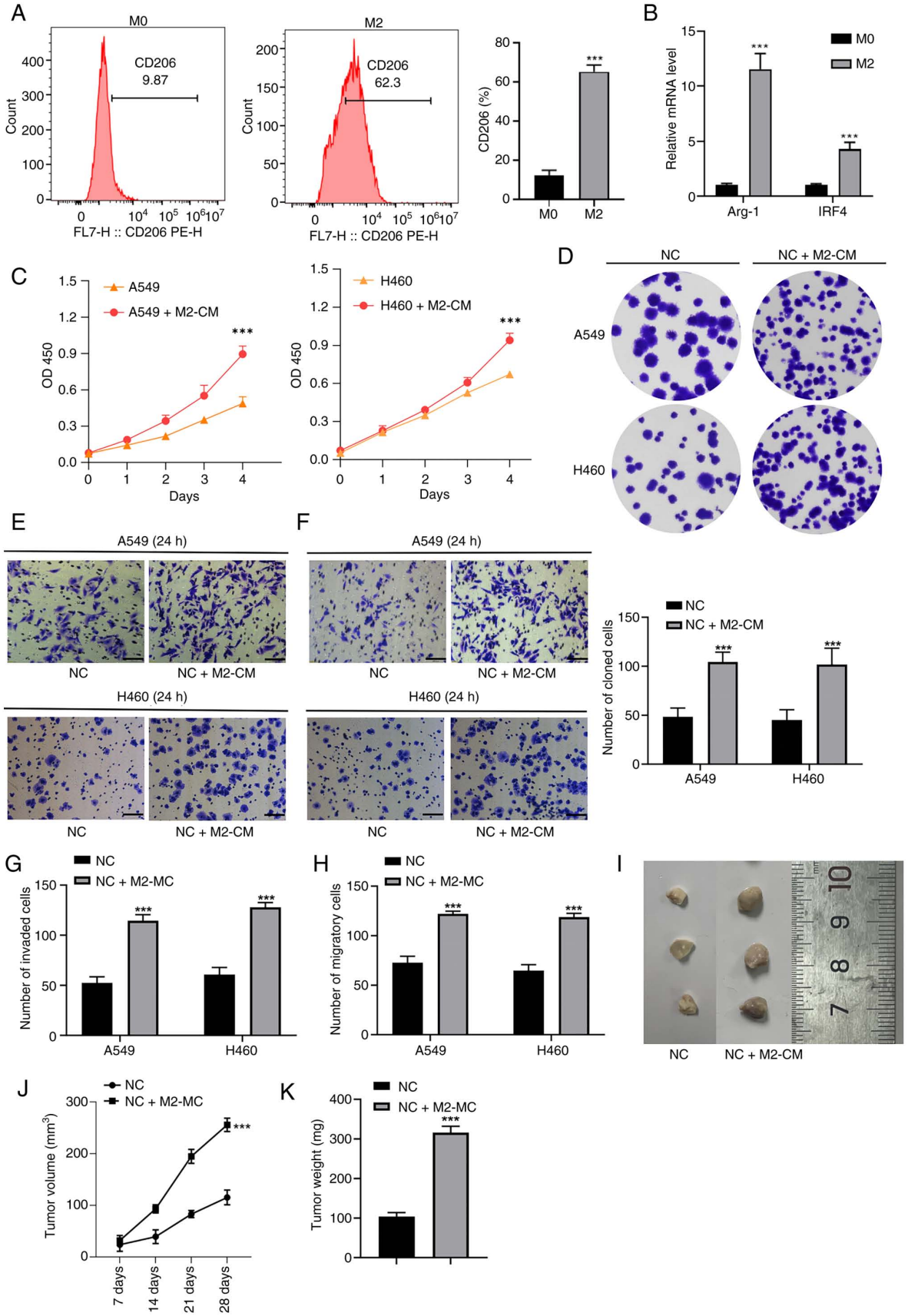

Figure 2. M2-like macrophages promote proliferation, migration, and invasion of lung cancer cells. (A) Flow cytometric analysis of CD206 expression in M0 and M2-like macrophages. (B) ARG1 and IRF4 gene expression in M0 and M2-like macrophages. (C) Proliferation curves of A549 and H460 lung cancer cells treated with or without M2-CM. (D) Colony formation assays of A549 and H460 lung cancer cells treated with or without M2-CM. (E) Migration assays (24 h) of A549 and H460 cells treated with or without M2-CM. Scale bar, 100 μm. (F) Invasion assays (24 h) of A549 and H460 cells treated with or without M2-CM. Scale bar, 100 μm. (G) Quantitative analysis of cell invasion. (H) Quantitative analysis of cell migration. (I) Subcutaneous tumor implantation of A549 cells with or without M2-CM treatment. (J) Tumor volume changes in mice implanted with A549 cells with or without M2-CM treatment. (K) Tumor weight of A549 xenografts with or without M2-CM treatment. Data are presented as mean ± SD. ***P<0.001. CM, conditioned medium.

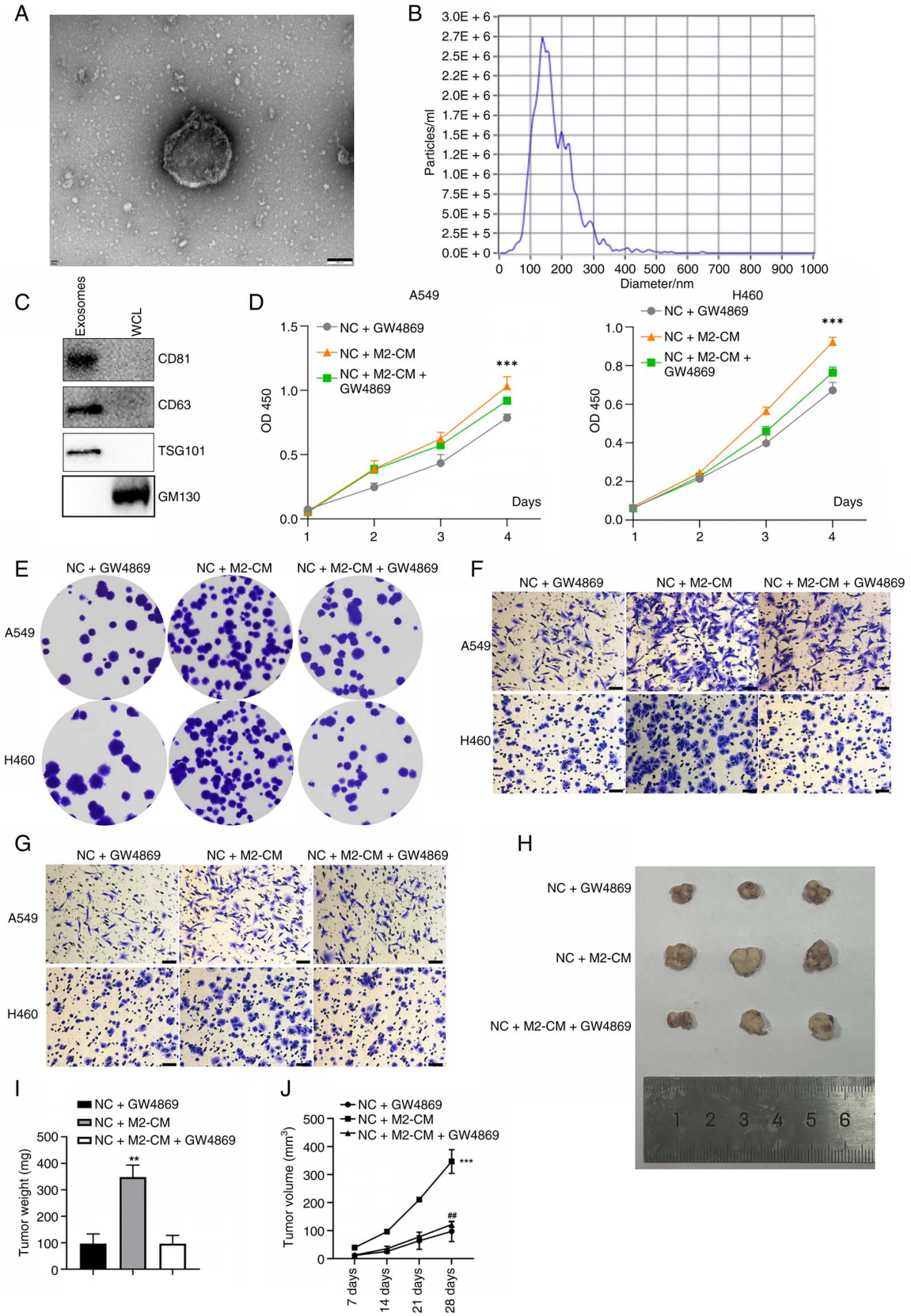

Figure 3. M2-like macrophages facilitate proliferation, migration, and invasion of lung cancer cells via exosomes. (A) TEM images showing exosome morphology. Scale bar, 100 nm. (B) NTA analysis of exosome diameter distribution. (C) Western blotting of CD81, CD63, TSG101 and GM130 in exosomes and whole-cell lysates. (D) Proliferation curves for A549 and H460 cells treated with CM, M2-CM, or M2-CM plus GW4869. (E) Colony formation assays for A549 and H460 cells treated with control medium, M2-CM, or M2-CM plus GW4869. (F) Migration assays of A549 and H460 cells treated with CM, M2-CM, or M2-CM plus GW4869. Scale bar, 100 μm. (G) Invasion assays of A549 and H460 cells treated with CM, M2-CM, or M2-CM plus GW4869. Scale bar, 100 μm. (H) Representative images of subcutaneous tumors derived from A549 cells treated with CM, M2-CM, or M2-CM plus GW4869. (I) Tumor weights in mice implanted with A549 and H460 cells treated with CM, M2-CM, or M2-CM plus GW4869. (J) Tumor volume changes in mice implanted with A549 and H460 cells treated with control medium, M2-CM, or M2-CM plus GW4869. Data are presented as mean ± SD. **P<0.01, ***P<0.001. TEM, transmission electron microscopy; NTA, nanoparticle tracking analysis; CM, conditioned medium.

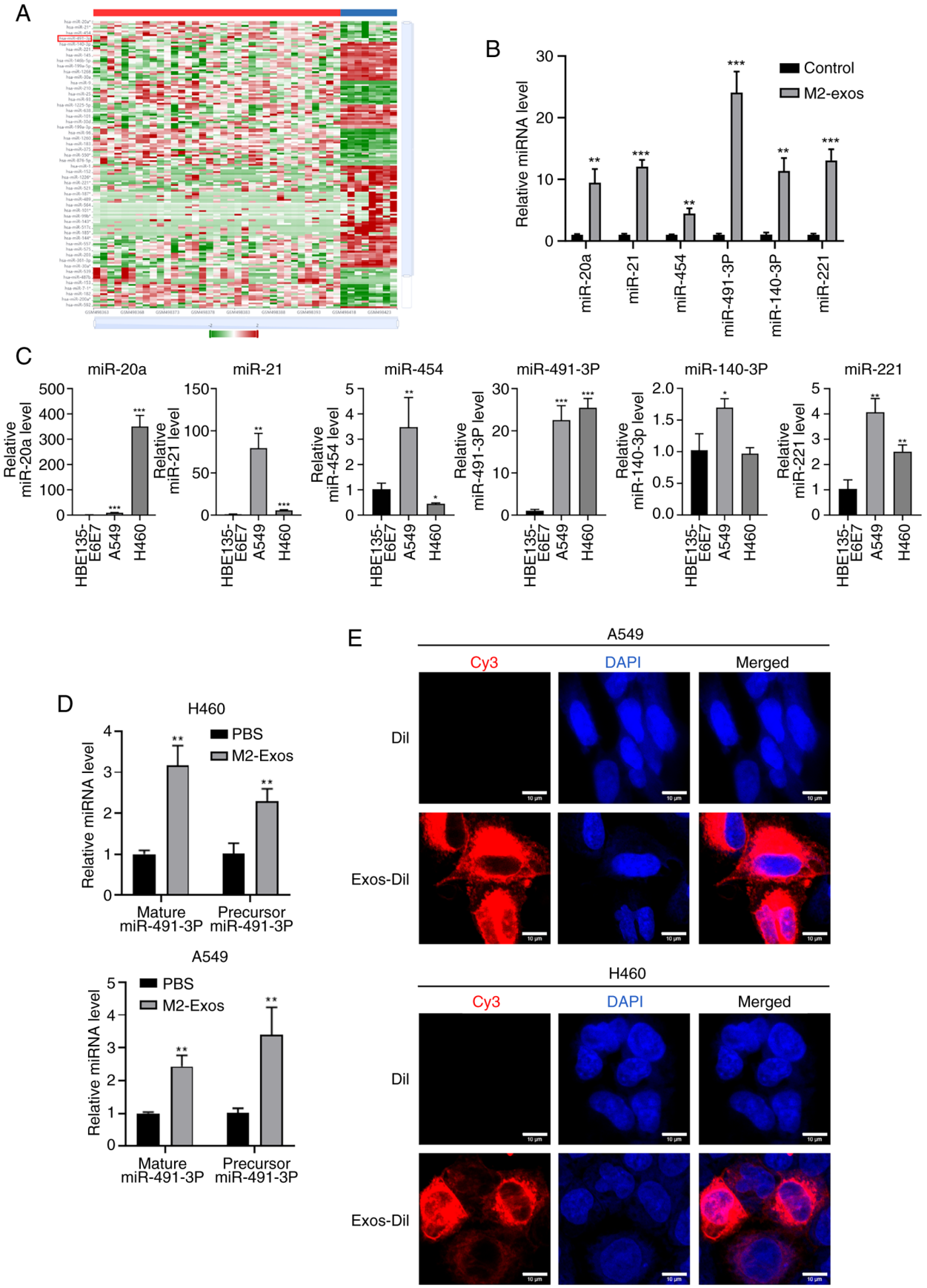

Figure 4. M2-like macrophages release exosomes enriched in miR-491-3p affecting lung cancer cells. (A) Heatmap of differentially expressed miRNAs regulating lung cancer progression from the GEO database. (B) Expression levels of miR-20a, miR-21, miR-454, miR-491-3p, miR-140-3p, and miR-221 between control (medium-only) and exosomes derived from M2-like macrophages. (C) Expression levels of miR-20a, miR-21, miR-454, miR-491-3p, miR-140-3p and miR-221 in HBE135-E6E7, A549 and H460 cells. (D) Expression levels of precursor and mature miR-491-3p in A549 and H460 cells. (E) Schematic diagram illustrating that DiI-labeled exosomes from M2-like macrophages are internalized by A549 and H460 lung cancer cells. Scale bar, 10 μm. Data are presented as mean ± SD. *P<0.05, **P<0.01, ***P<0.001. miR/miRNAs, microRNAs; GEO, Gene Expression Omnibus.

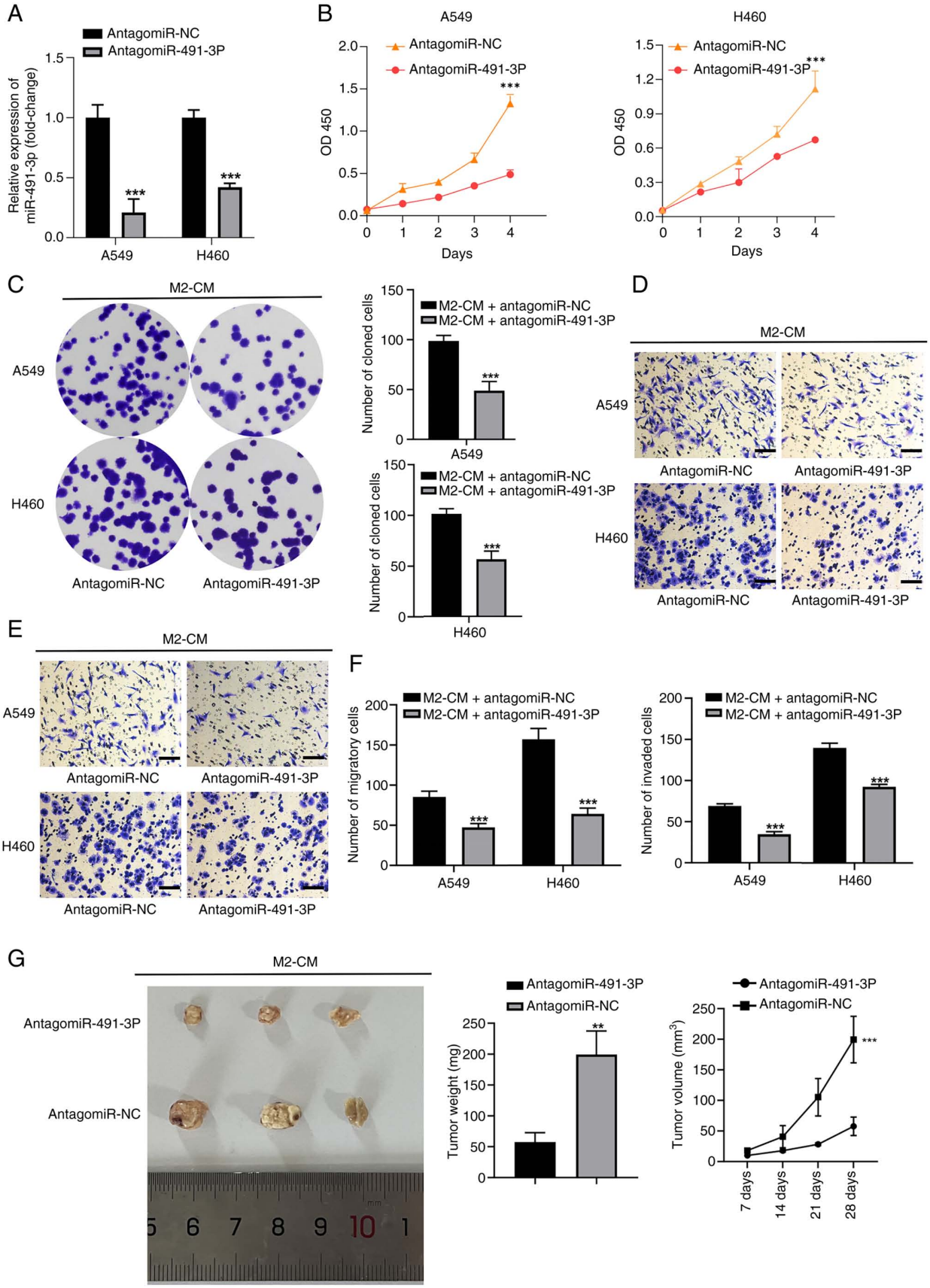

Figure 5. Inhibition of miR-491-3p attenuates lung cancer progression. (A) Verification of reduced miR-491-3p expression after transfection with antagomiR-491-3p. (B) Proliferation curves of A549 and H460 cells in antagomiR-NC and antagomiR-491-3p groups. (C) Colony formation and quantitative analysis of A549 and H460 cells in antagomiR-NC and antagomiR-491-3p groups. (D) Migration assays of A549 and H460 cells in antagomiR-NC and antagomiR-491-3p groups. Scale bar, 100 μm. (E) Invasion assays of A549 and H460 cells in antagomiR-NC and antagomiR-491-3p groups. Scale bar, 100 μm. (F) Quantitative analysis of migration and invasion in A549 and H460 cells. (G) Subcutaneous tumor formation, tumor weight and tumor volume in mice implanted with A549 cells from antagomiR-NC and antagomiR-491-3p groups. Data are presented as mean ± SD. **P<0.01, ***P<0.001. miR/miRNAs, microRNAs; NC, negative control.

Table I. Top 10 predicted downstream target genes of miR-491-3p in the TargetScan database.

Target Rank	Target Score	miRNA Name	Gene Symbol	Gene Description
1	99	miR-491-3p	UBE2D3	ubiquitin conjugating enzyme E2 D3
2	99	miR-491-3p	PCDH7	protocadherin 7
3	98	miR-491-3p	SLC5A7	solute carrier family 5 member 7
4	98	miR-491-3p	PCGF5	polycomb group ring finger 5
5	98	miR-491-3p	AZI2	5-azacytidine induced 2
6	97	miR-491-3p	PTPRM	protein tyrosine phosphatase, receptor type M
7	97	miR-491-3p	GNPTG	N-acetylglucosamine-1-phosphate transferase subunit gamma
8	97	miR-491-3p	EEA1	early endosome antigen 1
9	96	miR-491-3p	BNC2	basonuclin 2
10	96	miR-491-3p	RBM46	RNA binding motif protein 46

normal tissues (Fig. 6C). Following antagomiR-491-3p treatment, UBE2D3 expression markedly increased in tumor cells, suggesting a negative regulatory relationship between miR-491-3p and UBE2D3 (Fig. 6D). A ROC curve analysis produced an AUC of 0.8842, indicating markedly reduced UBE2D3 expression in tumor tissues (Fig. 6E). Suppressing miR-491-3p expression led to decreased colony formation, migration, and invasion in lung cancer cells. To further investigate this mechanism, UBE2D3 knockdown using shRNA partially reversed the inhibitory effects of miR-491-3p suppression, restoring colony formation, migration, and invasion capabilities in lung cancer cells (Fig. 6F-H). These findings collectively demonstrated that miR-491-3p promotes lung cancer progression by inhibiting UBE2D3 expression.

Discussion

Tumor progression and evolution result from interactions among multiple factors, with the TME playing a critical role (19,20). Exosomes represent a pivotal link between tumor and non-tumor cells, performing essential regulatory functions. TAMs are closely associated with tumor initiation and advancement (21,22). Within the TME, TAMs regulate immune responses, promote angiogenesis, control tissue remodeling, and facilitate invasion and metastasis (23,24). Thus, clarifying the molecular mechanisms underlying exosome-mediated communication between tumor and non-tumor cells is vital. Such understanding can elucidate complex regulatory networks and guide innovative therapeutic strategies, including exosome inhibition, reversal of immunosuppressive microenvironments and mitigation of drug resistance.

The present study demonstrated that M2-like macrophages release exosomes rich in miR-491-3p, which promote lung cancer progression upon uptake by tumor cells. Given the oncogenic role of miR-491-3p in lung cancer, targeting this molecule represents a promising therapeutic approach, providing a valuable theoretical foundation for drug development. As well as miRNAs, exosomes can deliver proteins, lncRNAs and circRNAs. For example, M2 TAM-derived exosomes containing MALAT1 enhance aerobic glycolysis in gastric cancer cells, thereby increasing proliferation, invasion, metastasis and chemoresistance in a glycolysis-dependent manner (25). Typically, signaling between tumor cells and M2 TAMs is bidirectional. Breast cancer cells release exosomes enriched with lncRNA HAGLROS, promoting M2 macrophage polarization and tumor progression (26). Likewise, gastric cancer cells deliver circATP8A1 to macrophages via exosomes, accelerating M2 polarization and tumor growth. Collectively, these findings highlight the critical regulatory role of M2 TAMs in tumor development (27).

M2-TAMs are established as tumor-promoting macrophages, whereas M1-TAMs inhibit tumor growth (28). Considering their distinct biological functions, cellular engineering technologies provide novel possibilities for cancer treatment by transforming M2-TAMs into M1-TAMs. Combining TLR agonists and interferon-γ markedly reprogrammed M2 into M1 macrophages in Lewis lung cancer models (29). TLR7/8 agonists (such as ruximod and R848) effectively converted M2-TAMs into M1-TAMs, demonstrating anti-tumor effects (30). Moreover, disrupting interactions between M2-TAMs and tumor cells is equally important. Traditional Chinese medicine (such as Dahuang Zhechong Wan) reduces CCL2 expression in CRC-derived exosomes, inhibits M2 polarization mediated by CCL2, improves the tumor immune microenvironment and suppresses CRC liver metastasis (31). Although research on M2-TAM-tumour cell communication is relatively comprehensive, developing therapeutic agents to block these interactions remains challenging and requires long-term efforts.

UBE2D3 serves as a key regulatory target for miR-491-3p in lung cancer cells, markedly affecting tumor progression. Existing research indicates that UBE2D3 displays tissue-specific effects across tumor types. Elevated UBE2D3 expression promotes tumor proliferation in pancreatic cancer and gliomas (32,33), but is notably decreased in esophageal cancer (34). The tissue specificity of UBE2D3 complicates its clinical translation as a lung cancer therapeutic target. Conversely, targeting miR-491-3p within the miR-491-3p-UBE2D3 signaling axis has greater therapeutic potential. Preventing miR-491-3p uptake into lung cancer cells represents a promising approach to inhibit tumor progression, offering substantial clinical potential.

The present study elucidated the molecular mechanisms by which M2-like macrophages promote lung cancer progression.

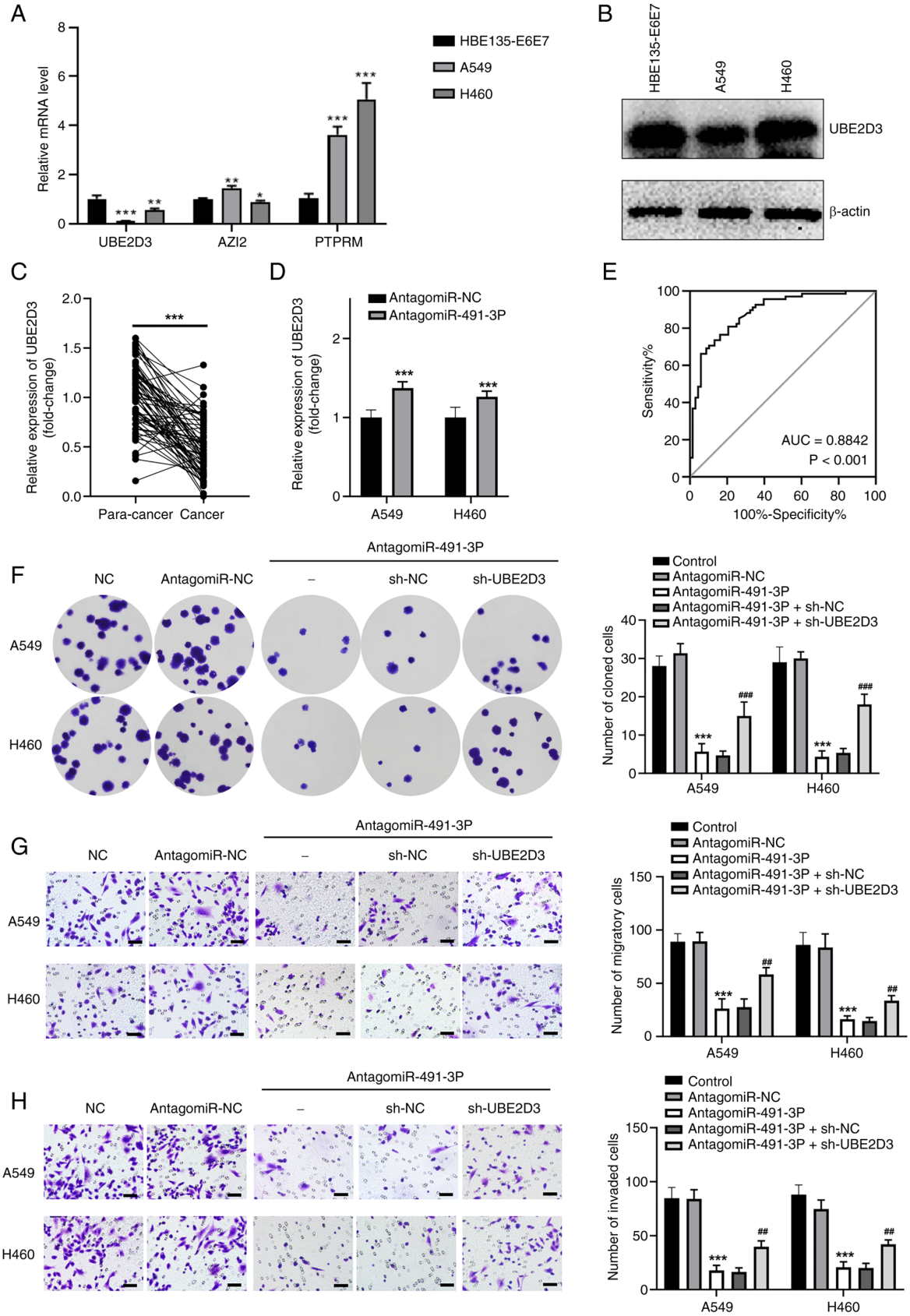

Figure 6. miR-491-3p promotes lung cancer progression by inhibiting UBE2D3 expression. (A) mRNA expression of UBE2D3, AZI2, and PTPRM in HBE135-E6E7, A549, and H460 cells. (B) Western blotting of UBE2D3 protein expression in HBE135-E6E7, A549, and H460 cells. (C) mRNA levels of UBE2D3 in 68 paired clinical lung cancer tissues and adjacent normal tissues. (D) mRNA expression levels of UBE2D3 in A549 and H460 cells treated with antagomiR-NC or antagomiR-491-3p. (E) ROC curve analysis for UBE2D3 expression in lung cancer tissues. (F) Colony formation and quantitative analysis of A549 and H460 cells treated with control, antagomiR-491-3p, and antagomiR-491-3p+sh-UBE2D3. (G) Migration assays and quantitative analysis in A549 and H460 cells treated with control, antagomiR-491-3p, and antagomiR-491-3p+sh-UBE2D3. Scale bar, 100 μm. (H) Invasion assays and quantitative analysis in A549 and H460 cells treated with control, antagomiR-491-3p and antagomiR-491-3p+sh-UBE2D3. Scale bar, 100 μm. Data are presented as mean ± SD. *P<0.05, **P<0.01, ***P<0.001, $^{\#\#}$P<0.01, $^{\#\#\#}$P<0.001. miR/miRNAs, microRNAs; NC, negative control; ROC, receiver operating characteristic; sh, short hairpin.

M2-like macrophages secrete exosomes enriched with miR-491-3p that influence lung cancer cells. Upon uptake by cancer cells, these exosomes modulate the expression of the UBE2D3 gene, thereby promoting tumor cell proliferation, migration, and invasion and ultimately accelerating disease progression. Several limitations exist in the present study. First, it did not quantitatively measure changes in exosome abundance using NTA following GW4869 treatment. Second, it relied solely on GW4869 for exosomes inhibition without employing alternative validation methods, such as uptake blockade or SEC-based purification. Finally, in the exosome uptake experiments, quantitative evaluation by orthogonal methodologies was not performed. Despite these limitations, the findings highlighted critical signaling interactions between tumor and non-neoplastic cells within the TME, suggesting potential therapeutic targets for lung cancer intervention.

Acknowledgements

Not applicable.

Funding

The present study was supported by a key project of Nanjing Medical Technology Development Fund (grant no. ZKX19046).

Availability of data and materials

The data generated in the present study may be requested from the corresponding author.

Authors' contributions

Conceptualization was by QZ, YS and XZ. Organizing and annotating the experimental data was by QZ, YS, YZ, SJ and SX. Formal analysis was by QZ, YS, SJ and SX; Funding acquisition was by FS. Investigation was by QZ, YS and XZ. Methodology was by QZ, MY, QW, WZ and XZ. Project administration was by FS and XZ. Resources were from QZ, FS and XZ. Software was by QZ and SX. Supervision was by FS and XZ. Validation was by QZ and XZ. Visualization was by SX. Writing the original draft was by QZ and SX. Writing, review and editing was by QZ and XZ. QZ and XZ confirm the authenticity of all the raw data. All authors read and approved the final manuscript.

Ethics approval and consent to participate

The present study was approved by the Ethics Committee of the Department of Thoracic Surgery at Nanjing Chest Hospital. All participants signed informed consent forms prior to participation and agreed to the publication of this article (approval no. 2023-KL034-01). The animal experiments were approved by the Animal Ethics Committee of Jiangnan University [approval no. JN.No20241230b0200211(715)].

Patient consent for publication

Not applicable.

Competing interests

The authors declare that they have no competing interests.

References

1. Shi X, Wang X, Yao W, Shi D, Shao X, Lu Z, Chai Y, Song J, Tang W and Wang X: Mechanism insights and therapeutic intervention of tumor metastasis: Latest developments and perspectives. Signal Transduct Target Ther 9: 192, 2024.
2. Kabakov A, Yakimova A and Matchuk O: Molecular chaperones in cancer stem cells: Determinants of stemness and potential targets for antitumor therapy. Cells 9: 892, 2020.
3. Yang Y, Ma X, Li Y, Jin L and Zhou X: The evolving tumor-associated adipose tissue microenvironment in breast cancer: From cancer initiation to metastatic outgrowth. Clin Transl Oncol 27: 2778-2788, 2025.
4. Zellmer VR and Zhang S: Evolving concepts of tumor heterogeneity. Cell Biosci 4: 69, 2014.
5. de Visser KE and Joyce JA: The evolving tumor microenvironment: From cancer initiation to metastatic outgrowth. Cancer Cell 41: 374-403, 2023.
6. Prakash J and Shaked Y: The interplay between extracellular matrix remodeling and cancer therapeutics. Cancer Discov 14: 1375-1388, 2024.
7. Bejarano L, Jordão MJC and Joyce JA: Therapeutic targeting of the tumor microenvironment. Cancer Discov 11: 933-959, 2021.
8. Noy R and Pollard JW: Tumor-associated macrophages: From mechanisms to therapy. Immunity 41: 49-61, 2014.
9. Mantovani A and Allavena P: The interaction of anticancer therapies with tumor-associated macrophages. J Exp Med 212: 435-445, 2015.
10. Sun X, Gao D, Gao L, Zhang C, Yu X, Jia B, Wang F and Liu Z: Molecular imaging of tumor-infiltrating macrophages in a preclinical mouse model of breast cancer. Theranostics 5: 597-608, 2015.
11. Kalluri R and LeBleu VS: The biology, function, and biomedical applications of exosomes. Science 367: eaau6977, 2020.
12. Guo W, Li Y, Pang W and Shen H: Exosomes: A potential therapeutic tool targeting communications between tumor cells and macrophages. Mol Ther 28: 1953-1964, 2020.
13. Xu Z, Chen Y, Ma L, Chen Y, Liu J, Guo Y, Yu T, Zhang L, Zhu L and Shu Y: Role of exosomal non-coding RNAs from tumor cells and tumor-associated macrophages in the tumor microenvironment. Mol Ther 30: 3133-3154, 2022.
14. Boelens MC, Wu TJ, Nabet BY, Xu B, Qiu Y, Yoon T, Azzam DJ, Twyman-Saint Victor C, Wiemann BZ, Ishwaran H, *et al*: Exosome transfer from stromal to breast cancer cells regulates therapy resistance pathways. Cell 159: 499-513, 2014.
15. Romano R, Picca A, Eusebi LHU, Marzetti E, Calvani R, Moro L, Bucci C and Guerra F: Extracellular vesicles and pancreatic cancer: Insights on the roles of miRNA, lncRNA, and protein cargos in cancer progression. Cells 10: 1361, 2021.
16. Xie Y, Dang W, Zhang S, Yue W, Yang L, Zhai X, Yan Q and Lu J: The role of exosomal noncoding RNAs in cancer. Mol Cancer 18: 37, 2019.
17. Han C, Zhang C, Wang H and Zhao L: Exosome-mediated communication between tumor cells and tumor-associated macrophages: Implications for tumor microenvironment. Oncoimmunology 10: 1887552, 2021.
18. Théry C, Witwer KW, Aikawa E, Alcaraz MJ, Anderson JD, Andriantsitohaina R, Antoniou A, Arab T, Archer F, Atkin-Smith GK, *et al*: Minimal information for studies of extracellular vesicles 2018 (MISEV2018): A position statement of the international society for extracellular vesicles and update of the MISEV2014 guidelines. J Extracell Vesicles 7: 1535750, 2018.
19. Yuan Y, Jiang YC, Sun CK and Chen QM: Role of the tumor microenvironment in tumor progression and the clinical applications (review). Oncol Rep 35: 2499-2515, 2016.
20. Wang Q, Shao X, Zhang Y, Zhu M, Wang FXC, Mu J, Li J, Yao H and Chen K: Role of tumor microenvironment in cancer progression and therapeutic strategy. Cancer Med 12: 11149-11165, 2023.
21. Yang E, Wang X, Gong Z, Yu M, Wu H and Zhang D: Exosome-mediated metabolic reprogramming: The emerging role in tumor microenvironment remodeling and its influence on cancer progression. Signal Transduct Target Ther 5: 242, 2020.

22. Su T, Zhang P, Zhao F and Zhang S: Exosomal MicroRNAs mediating crosstalk between cancer cells with cancer-associated fibroblasts and tumor-associated macrophages in the tumor microenvironment. Front Oncol 11: 631703, 2021.
23. Dallavalasa S, Beeraka NM, Basavaraju CG, Tulimilli SV, Sadhu SP, Rajesh K, Aliev G and Madhunapantula SV: The role of tumor associated macrophages (TAMs) in cancer progression, chemoresistance, angiogenesis and metastasis-current status. Curr Med Chem 28: 8203-8236, 2021.
24. Fu LQ, Du WL, Cai MH, Yao JY, Zhao YY and Mou XZ: The roles of tumor-associated macrophages in tumor angiogenesis and metastasis. Cell Immunol 353: 104119, 2020.
25. Wang Y, Zhang J, Shi H, Wang M, Yu D, Fu M, Qian Y, Zhang X, Ji R, Wang S, *et al*: M2 tumor-associated macrophages-derived exosomal MALAT1 promotes glycolysis and gastric cancer progression. Adv Sci (Weinh) 11: e2309298, 2024.
26. Meng Z, Zhang R, Wu X, Piao Z, Zhang M and Jin T: LncRNA HAGLROS promotes breast cancer evolution through miR-135b-3p/COL10A1 axis and exosome-mediated macrophage M2 polarization. Cell Death Dis 15: 633, 2024.
27. Deng C, Huo M, Chu H, Zhuang X, Deng G, Li W, Wei H, Zeng L, He Y, Liu H, *et al*: Exosome circATP8A1 induces macrophage M2 polarization by regulating the miR-1-3p/STAT6 axis to promote gastric cancer progression. Mol Cancer 23: 49, 2024.
28. Zhang W, Wang M, Ji C, Liu X, Gu B and Dong T: Macrophage polarization in the tumor microenvironment: Emerging roles and therapeutic potentials. Biomed Pharmacother 177: 116930, 2024.
29. Müller E, Christopoulos PF, Halder S, Lunde A, Beraki K, Speth M, Øynebråten I and Corthay A: Toll-like receptor ligands and interferon-γ synergize for induction of antitumor M1 macrophages. Front Immunol 8: 1383, 2017.
30. Figueiredo P, Lepland A, Scodeller P, Fontana F, Torrieri G, Tiboni M, Shahbazi MA, Casettari L, Kostiainen MA, Hirvonen J, *et al*: Peptide-guided resiquimod-loaded lignin nanoparticles convert tumor-associated macrophages from M2 to M1 phenotype for enhanced chemotherapy. Acta Biomater 133: 231-243, 2021.
31. Chen C, Yao X, Xu Y, Zhang Q, Wang H, Zhao L, Wen G, Liu Y, Jing L and Sun X: Dahuang Zhechong pill suppresses colorectal cancer liver metastasis via ameliorating exosomal CCL2 primed pre-metastatic niche. J Ethnopharmacol 238: 111878, 2019.
32. Wang S, Yang W, Peng T, Zhu C, Dong J, Wang Y, Yuan H, Sun Q, Luan X, Guan X, *et al*: IFN-γ-driven UBE2D3 upregulation impairs antigen presentation pathways and anti-tumor immunity in pancreatic cancer. Nat Commun 16: 10733, 2025.
33. Pan Z, Bao J, Zhang L and Wei S: UBE2D3 activates SHP-2 ubiquitination to promote glycolysis and proliferation of glioma via regulating STAT3 signaling pathway. Front Oncol 11: 674286, 2021.
34. Guan GG, Wang WB, Lei BX, Wang QL, Wu L, Fu ZM, Zhou FX and Zhou YF: UBE2D3 is a positive prognostic factor and is negatively correlated with hTERT expression in esophageal cancer. Oncol Lett 9: 1567-1574, 2015.